Available online at www.sciencedirect.com

SciVerse ScienceDirect

Journal of the European Ceramic Society 34 (2014) 1–11

www.elsevier.com/locate/jeurceramsoc

Rare-earth modified zirconium diboride high emissivity coatings for hypersonic applications

Winnie Tan [a], Christopher A. Petorak [b], Rodney W. Trice [a,*]

[a] *Purdue University, West Lafayette, IN 47907, USA*
[b] *Praxair Surface Technologies Inc., Indianapolis, IN 46222, USA*

Received 30 May 2013; received in revised form 12 July 2013; accepted 17 July 2013
Available online 22 August 2013

Abstract

Sharp features of hypersonic vehicles increases heat transfer to the surface during flight. This thermal energy can be reduced via increasing the radiation and conduction heat transfer away from the surface. In this study, an emissivity modifier was incorporated into an ultra-high-temperature-ceramic coating system (ZrB_2/SiC) to increase its surface radiation heat transfer rate by increasing the emissivity of the surface. The rare-earth were incorporated into the coatings via mechanical mixing Sm_2O_3 or Tm_2O_3 with ZrB_2/SiC or chemically infiltrating $Sm(NO_3)_3$/ethanol solution into ZrB_2/SiC. Coatings were fabricated using shrouded air plasma spray. Total hemispherical emissivity results show that the $Sm(NO_3)_3$ infiltrated ZrB_2/SiC coating had a higher emissivity compared to the baseline ZrB_2/SiC coatings up to 1200 °C. The thermal conductivity of all coatings presently studied was below 12 W/m/K. The presence of rare-earth in the boria-rich surface glasses formed during oxidation increases the glass evaporation rate of the coatings compared to the ZrB_2/SiC coating.

Keywords: Thermal protection systems; Emissivity; Rare-earth oxides; Zirconium diboride; Plasma spray

1. Introduction

In next generation hypersonic vehicles, blunt leading edges will be replaced with sharp profiles to reduce aerodynamic drag and improve performance. As a consequence of this design change, their aerodynamic heating rate is also drastically increased,[1] with leading edge materials required to withstand very high temperatures for extended times. Ultra high temperature ceramics (UHTCs), such as ZrB_2 and HfB_2, are explored for this application because of their oxidation and ablation resistant properties.[2] Studies have shown that ZrB_2 with an additional 20–30 vol.% SiC secondary phase has the best oxidation performance, where the SiC forms a protective silicon oxide glass on the surface upon oxidation to extend the maximum operating temperature.[3]

During high-speed flight, a large amount of energy is being transferred into the system from the surface via convection and chemical heating.[4] Convection heating arises from the high enthalpy bow shock layer surrounding the sharp structures. At speeds of Mach 5 and above, the diatoms in the air such as N_2 and O_2 will dissociate into ions. These ions will recombine on the hot structure to release energy; hence chemically heating the surface.[4] Thermal energy can be removed from the surface via two mechanisms. A leading edge with high thermal conductivity is desirable because it reduces the thermal gradient within the system and mitigates the effect of local hot spots.[5] While thermal conduction helps to distribute the heat in the leading edge, radiation heat transfer has the ability to re-radiate the heat away from the system, resulting in a lower surface temperature on the leading edge.

The material property that determines the amount of radiation heat transfer is emissivity, ε. A high emissivity is desired to maximize the amount of heat radiated from the surface. Van Wei et al. developed a radiation equilibrium approach to calculate the wall temperature of a hypersonic vehicle surface. In their study, they demonstrated the importance of having a high emissivity surface on the leading edge to reduce its temperature. For example, at a pressure of 0.24 atm and a speed of Mach 10, surfaces with an emissivity of 0.5 and 1.0 have a surface temperature of

* Corresponding author at: 701 West Stadium Avenue, West Lafayette, IN 47907, USA. Tel.: +1 765 494 6405; fax: +1 765 494 1204.
E-mail address: rtrice@purdue.edu (R.W. Trice).

0955-2219/$ – see front matter © 2013 Elsevier Ltd. All rights reserved.
http://dx.doi.org/10.1016/j.jeurceramsoc.2013.07.016

2400 °C and 2100 °C, respectively.[1] Furthermore, Guazzoni and Alfano et al. state that radiation heat transfer is the only method for heating and cooling in outer space applications.[6,7] Clearly, optimizing radiation heat transfer can make a significant difference in reducing leading edge temperature, but few studies have been performed to understand the radiation properties of high temperature materials.[8]

An ideal material system for hypersonic applications requires a melting temperature of 1500 °C and above, high thermal conductivity, high emissivity, and low chemical reactivity.[7,8] Rare-earth oxides (REO) meet the above criteria. Not only do they have melting temperatures greater than 2200 °C, they also have low chemical reactivity with the environment. High emissivity over a broad temperature range is desirable because the system is able to redistribute heat, reduce surface temperature, and chemical reaction rates.[7] Studies indicate that Sm_2O_3, Er_2O_3, Tm_2O_3, and Nd_2O_3 have high average emittance values overoptical and infrared wavelengths (0.5–5.0 μm).[6,9] In particular, samarium and thulium oxides have similar f-shell absorption bands, causing the two to have similar optical performance.[10] Total hemispherical emissivity, where emittance is integrated over all wavelengths and all directions, is the best indicator to quantify surface emissivity. While the REOs mentioned have the requisite high emissivity, they also possess coefficient of thermal expansions that are 20–30% larger than ZrB_2/SiC.[11,12] Thus, a composite coating containing ZrB_2/SiC and REO is an attractive approach as the majority phase of the coating is the same as the underlying ZrB_2/SiC structure.

Finally, conventional air plasma spray is not an acceptable fabrication method to prepare ZrB_2/SiC coatings. Preliminary x-ray diffraction studies of ZrB_2 prepared by conventional air plasma spray revealed that all ZrB_2 powder oxidized to *m*-ZrO_2. Tului et al. patented an inert gas plasma spray process to create ZrB_2/SiC coatings, which also demonstrated that the oxidation behavior of such coatings is very similar to the sintered ZrB_2-SiC system, despite their very different microstructures.[13,14] The major plasma spray technique used in this project is the shrouded air plasma spray (APS) using a proprietary process developed by Praxair Surface Technologies. This spraying technique provides a faster process time and reduces production cost compared to vacuum or inert gas plasma spray.[15]

In the work reported currently we have modified the emissivity of ZrB_2/SiC coatings via the addition of rare-earth additives using two approaches. In the first approach, 23 vol.% (10 mol.%) of either Sm_2O_3 or Tm_2O_3 powders were added to spray-dried ZrB_2 powders. In the second approach, 20 mol% $Sm(NO_3)_3$ dissolved in ethanol was infiltrated into the porous spray-dried ZrB_2 powders and the solvent was evaporated. In both approaches, 20 vol.% SiC was added to the spray-dried mixtures prior to shrouded air plasma spraying. The microstructure and physical properties of these coatings, including total hemispherical emissivity, thermal conductivity and oxidation resistance are described in this paper.

2. Experimental procedure

2.1. Powder preparation and formulation

A lab spray dryer (APV Anhydro Model S1, Anhydro Inc, Soeborg, Denmark) was used to produce powder agglomerate from a liquid feed. (Aero-Instant Spraying Service, Brunswick, USA) The suspension consisted of 50 vol.% ZrB_2(Grade B, HC Starck, Munich, Germany), DI water, 0.15 wt% dispersant (Darvan 821 A, R. T. Vanderbilt Company, Inc., Norwalk, USA) and 2 wt% PVA binder (Celvol 203, Celanese Corporation, Dallas, USA). The suspension was fed into the drying chamber via a spraying nozzle, where the air was heated to 200 °C. A rotary atomizer spun at ~30,000 rpm to atomize the suspension into controlled-size droplets. The temperature at the outlet was approximately 105 °C. The average particle size of the spray-dried powder was analyzed by a Malvern Mastersizer 2000(Malvern Instrument Ltd., Worcestershire, UK), and was approximately 38 μm using a reflective index of 1.92.

Two types of rare-earth elements and two mixing approaches were investigated. In the first approach, spray dried ZrB_2, SiC (Grade UF-10, HC Starck, Munich, Germany), and either Sm_2O_3 or Tm_2O_3 powders (99.9% pure, American Elements, Los Angeles, USA), were dry-mixed (DM) in the desired proportions and roller milled to ensure homogeneous mixing. The chemical compositions of the two types of DM coatings are shown in Table 1.

In the second approach, the rare-earth dopant was added via a chemical-doping (DOP) approach by dissolving 20 mol% samarium nitrate, $Sm(NO_3)_3$ (99.9% pure, Sigma–Aldrich, St. Louis, USA) into 200-proof ethanol. The solution was then infiltrated into the spray-dried ZrB_2 powder and roller milled for 24 hours to ensure homogenous mixing. The mixture was next dried using a RotoVap (BM 200, Yamato Scientific America Inc., Santa Clara, USA) at 100 °C to remove the solvent. This powder was heat treated at 500 °C for 1 h to remove residual moisture and nitrates. The dried mixture was then sieved using a 325-mesh (44 μm) sieve to eliminate large agglomerates, and 20 vol.% SiC powders were added and mechanically mixed. The formulation of the DOP powder is listed in Table 1.

All coatings prepared currently contain the baseline materials, which were ZrB_2/20vol.% SiC, and are identified currently

Table 1
Chemical formulations of coatings prepared via shrouded air plasma spray.

vol% (mol%)	SiC	ZrB_2	Sm_2O_3	Tm_2O_3	$Sm(NO_3)_3{\cdot}6H_2O$
ZBS	20 (27.06)	80 (72.84)	–	–	–
SmZBS-DM	16.7 (24.35)	60.1 (65.65)	23.2 (10.00)	–	–
TmZBS-DM	16.8 (24.35)	60.5 (65.65)	–	22.7 (10)	–
SmZBS-DOP	20 (24.35)	80 (55.65)	–	–	(20)

as ZBS. To help simplify discussion, the following naming convention is used: rare earth type – baseline powder – mixing method. As an example, a SmZBS-DM coating is consisted of Sm_2O_3, spray-dried ZrB_2, and SiC powders, with the Sm_2O_3 added via the dry mix approach. Fumed silica (0.5 wt.%, Cab-O-Sil®, Cabot Corporation, Boston, USA) was added to all the powdersasa flowing agent for plasma spray.

2.2. Plasma spray process

The coatings were prepared at Praxair Surface Technologies (Indianapolis, USA) using a shrouded air plasma spray process. Their proprietary shroud design allowed plasma spraying at atmospheric pressures in inert gas without oxidation of ZrB_2 or SiC powders. The average coating thickness was approximately 200–350 μm.

2.3. Microstructural and phase analysis

Coating topography, cross section, and element analysis were observed using a scanning electron microscope (SEM) equipped with energy dispersive x-ray spectroscopy (EDS) (Phillips XL-40, FEI Co., Hillsboro, USA). The non-conductive ceramic coatings were coated with a thin layer of Au/Pd prior to imaging.

X-ray diffraction (XRD) using Cu K_α radiation (D8 Focus, Bruker Corporation, Billerica, USA) was performed on as-sprayed and oxidized coatings over 2θ values of 20–50°. A step size of 0.02° and a scan rate of 5°/min were used. The amount of samarium and silicon incorporated into the DM and DOP coatings was measured by mass spectroscopy techniques on pulverized coatings (NSL Analytical Services Inc., Cleveland, USA).

The surface roughness of the coatings were quantified with a profilometer (AS0200 AlphaStep, Tencor Corporation, Milpitas, USA) at a scan speed of 10 μm/s. A total length of 300 μm was measured for each coating. The density of the coatings was determined using Archimedes' methodology described in the ASTM C373-88 standard.[16] The theoretical density was calculated using the rule of mixtures approach based on final coating compositions, where the density of ZrB_2, SiC, Sm_2O_3, and Tm_2O_3 are 6.09 g/cm^3, 3.21 g/cm^3, 8.35 g/cm^3, and 8.60 g/cm^3, respectively.

2.4. Total hemispherical emissivity

Emissivity tests were performed by TPRL Inc. (West Lafayette, USA) using the ASTM C835-06 standard as a guide.[17] Electrically conductive tungsten rods with a 6 mm outer diameter were used as substrates. Approximately 20 μm of ZrB_2/SiC was applied to the W rod before applying the ~30 μm thick rare-earth modified ZrB_2/SiC coatings currently investigated. Prior to the emissivity test, two pairs of type-K thermocouples and a pair of platinum electrodes were spot welded onto the center region of the sample to obtain temperature and voltage readings, respectively. The emissivity as a function of temperature or $\varepsilon(T)$ was calculated according to:

$$\varepsilon(T) = \frac{i\Delta V}{PL\sigma(T^4 - T_o^4)} \quad (1)$$

where ΔV is the voltage drop measured from a voltmeter (V), I is the electric current (A), $P \times L$ is multiplication of perimeter and length of the test rod (m^2), σ is the Stefan–Boltzmann constant (W/m^{2}K^4), T and T_o are the sample and ambient temperatures (K). T_o is often negligible because it is relatively low compared to T.[8] This test is performed under a vacuum (<1.3 mPa) to ensure radiation is the sole heat transfer mechanism.

2.5. Thermal conductivity

Thermal diffusivity tests were performed at Oak Ridge National Laboratory-High Temperature Materials Laboratory (ORNL-HTML) using the laser flash technique. All samples were 12.5 mm diameter disks. A thin layer of colloidal graphite was deposited on both sides of the coatings to enhance the absorption of the applied energy.[18] Measurements were taken from 200 °C to 1000 °C at increments of 100 °C. An argon atmosphere was used for all thermal diffusivity measurements. At least two samples were tested for each coating. The thermal conductivity of each coating as a function of temperature or $k(T)$ was calculated using:

$$k(T) = D(T) \times \rho(T) \times c_p(T) \times 100 \quad (2)$$

where $D(T)$ is the measured thermal diffusivity (cm^2/s), $\rho(T)$ is coating density (g/cm^3), $c_p(T)$ is the specific heat of the coating (J/g K), with each quantity measured as a function of temperature. The densities of the coatings were measured at room temperature and the effect of temperature on coating densities was taken into account by considering their linear thermal expansions. The density as a function of temperature was calculated from:

$$\rho(T) = \rho_{RT}\left[\frac{\Delta l(T)}{l_{RT}}\right]^{-3} \quad (3)$$

where ρ_{RT} is measured density at room temperature (g/cm^3) and $(\Delta l(T)/l_{RT})$ is the linear thermal expansion.[12] The specific heats of coatings were obtained from the thermophysical properties of matter database (TPMD)[19] and calculated based on rules of mixture using mass fraction.

2.6. Oxidation test

Oxidation testing of the coatings was performed using thermogravimetry analysis (TGA) (SDT 1960, TA Instruments, New Castle, USA) with a 4.7 mm disk sample fitted into an alumina pan. In one test sequence, samples were heated at 5 °C/min from room temperature to 1300 °C in air. In the other test sequence, samples were heated in flowing nitrogen at 10 °C/min to the target temperature (900 °C, 1100 °C, or 1300 °C), then the atmosphere was switched to air and the weight gain was monitored for 2 h. Following completion of the test, air was replaced by

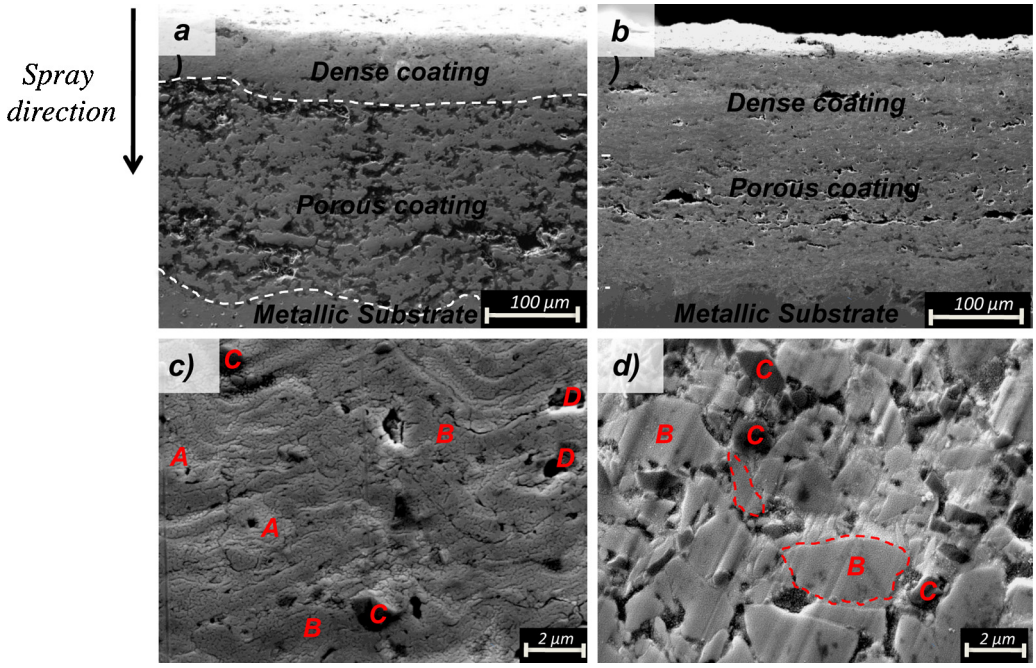

Fig. 1. Typical cross section of a plasma sprayed coating. (a) ZBS and (b) SmZBS-DM coatings show porosity changes with multiple plasma spray conditions. (c) High magnification SmZBS-DM microstructure shows individual lamellae. EDS analysis indicates areas with different contrast are (A) samarium-rich region; (B) ZrB_2 rich region; (C) SiC particle; and (D) pores. (d) SmZBS-DOP microstructure shows angular grains indicated by the dotted lines. They are fused together suggested incomplete melting in plasma plume before deposition.

nitrogen during cooling. Gas flow, whether nitrogen or air, was maintained at 100 sccm. All samples were stored in a desiccant after the test to prevent hydration of B_2O_3. The composition and topography of the oxidized coatings were observed by XRD and SEM, respectively.

3. Results and discussion

3.1. Characteristics of as-sprayed coatings

Fig. 1a and b shows typical SEM cross-sections in the baseline (ZBS) and SmZBS-DM coatings. There were regions in the coating that appeared porous and dense. A higher magnification SEM micrograph of SmZBS-DM coating (see Fig. 1c) reveals individual lamella formations, as is typically observed in plasma sprayed coatings.[15] EDS analysis indicated two types of lamellae: Sm_2O_3 and ZrB_2. The thin profile of each indicates complete melting prior to their striking on the substrate. The thickness of the lamellae is approximately 0.5–1 μm. Pores were observed between lamellae and there are spherical pores within a lamella. In contrast, angular SiC particles were observed, consistent with the fact that it does not melt. There are also micro-cracks formed perpendicular to the spray direction. TmZBS-DM coatings were similar to the SmZBS-DM coating but with Tm_2O_3 lamellae. The ZBS baseline coating has a similar microstructure to the two DM coatings, but without the Sm_2O_3 or Tm_2O_3 lamellae.

As shown in Fig. 1d the SmZBS-DOP coating was distinctively different from the SmZBS-DM coatings. The angular shape of both the ZrB_2 and SiC suggested that the powders were only partially melted during the plasma spray process. Consequently, the particles appear fused together with a large amount of porosity between each particle. The average ZrB_2 and SiC feature in the SmZBS-DOP coatings were very similar to the size of the starting powder – further indication that the powders were only partially melted.

The densities and porosities of all coatings are listed in Table 2. The two dry-mixed coatings, SmZBS-DM and TmZBS-DM, are 73–76% dense compared to the 58% dense SmZBS-DOP coating. The majority of the porosity was manifested as open porosity, which can strongly influence oxidation behavior. It should be noted that the spray parameters were not optimized for the coatings currently studied. In highly oxidizing environments like those experienced in hypersonic flight, dense coatings would be desired to prevent oxidation and maximize thermal conduction. It is well established that the microstructure of plasma-sprayed coatings can be improved by changing the spray parameters. For example, Pawlowski et al. shows that the ability of heating factor (AHF) for the plasma gun should exceed the difficulty of melting factor (DMF) to ensure all powders are fully melted in the plasma before deposition.[20] Tului et al. also describe the increase in coating hardness with AHF, where the inter-lamella cohesion is improved.[21]

As presented in Fig. 2, XRD analysis of Sm- or TmZBS-DM, SmZBS-DOP and baseline ZBS coatings in the as-sprayed condition showed ZrB_2 with no evidence of decomposition to *m*-ZrO_2. However, there was a small amorphous hump at low 2θ due to the small amount of SiO_2 added as a flowing agent to enable powder feeding into the plasma. Note that the XRD pattern from the starting ZrB_2/SiC powder is shown for comparison. Only minor amounts of SiC were present in all of the as-sprayed coatings as evidenced by low intensity peaks at 2θ of 35.5°. Peaks associated with the rare-earth oxide were

Table 2
Measured densities and porosities for the prepared coatings.

	Theoretical density[a] (g/cm^3)	Bulk density (g/cm^3)	Total porosity (%)	Open porosity (%)
ZBS	6.07	4.30	29.1	20.7
SmZBS-DM	6.44	4.68	27.3	20.2
TmZBS-DM	6.46	4.91	24.0	15.8
SmZBS-DOP	5.74	3.35	41.4	36.7

[a] Calculations performed based on the final coatings composition.

observed between 2θ ranging from 25 to 33° for SmZBS-DM and TmZBS-DM coatings. Mass spectroscopy results indicated that 15.5 vol.% Sm_2O_3 was successfully incorporated into SmZBS-DM coatings. There were no crystalline peaks associated with either pure samarium or Sm_2O_3 in the SmZBS-DOP coating. However, mass spectroscopy confirmed the presence of 10.3 vol.% Sm in the as-sprayed coating. For comparison purposes, if all the samarium in SmZBS-DOP had oxidized to Sm_2O_3 it would occupy 7.5 vol% of the composite. It is not clear in the present study where samarium is manifested within the coating but the subject is an ongoing investigation. In addition, less than 1.7 vol.% SiC was measured in the SmZBS-DM coating indicating that most of the SiC particles were lost during plasma spraying due to the fine particle size. Future modification of these processing approaches will include spray-drying SiC with ZrB_2 to form larger powder agglomerates.

3.2. Total hemispherical emissivity of plasma sprayed UHTC coatings

To establish repeatability for the total hemispherical emissivity test, the baseline ZBS sample was evaluated five times using the procedure described in Section 2.4. Each test consisted of the sample being heated to 1200 °C, cooled to room temperature, followed by reheating. The variations in the emissivity results averaged at each temperature were never greater than ±0.014. Furthermore, post-testing observations of the sample revealed no chemical reaction had occurred between the ZrB_2/SiC and W substrate.

The total hemispherical emissivity results of all coatings in the as-sprayed condition are presented in Fig. 3. The ZBS coating demonstrated decreasing emissivity, beginning with an emissivity of 0.9 at a temperature of 600 °C, to 0.77 at 875 °C, before increasing again to a value of 0.8 at 1200 °C. The DM samples, with similar emissivity values for both Sm_2O_3 or Tm_2O_3 additions, did not demonstrate the local minimum in emissivity for the temperatures investigated. The SmZBS-DOP coating demonstrated a local minimum in emissivity at 1050 °C before increasing to an emissivity of 0.93 at 1200 °C. In density function theory (DFT) simulations performed by Avdoshenko and Strachan,[22] this local minimum is associated with the transition from phonon to electron absorption. Unfortunately the total hemispherical emissivity tests on the two DM coatings ended at a temperature before the transition was observed. However, in the DM emissivity data, there appears to be a plateau in emissivity at 1050 °C similar to the plateau observed in the SmZBS-DOP sample just before the emissivity increase. Ultimately, further testing is required to find the exact transition temperatures for the two DM coatings.

The total hemispherical emissivity results indicated that the SmZBS-DOP coating has a distinctly higher emissivity compared to the ZBS coating and the two DM coatings investigated. One possible reason for this would be differences in surface roughness between the samples. In general, emissivity increases with surface roughness. Profilometer measurements of surface roughness, R_a, of the ZBS, SmZBS-DM, SmZBS-DOP, and TmZBS-DM coatings were 3.18 μm, 2.68 μm, 5.27 μm, and 3.19 μm, respectively. Clearly, the SmZBS-DOP surface roughness is twice as high as that of the SmZBS-DM coating, while the surface roughness of ZBS and TmZBS-DM are the same.

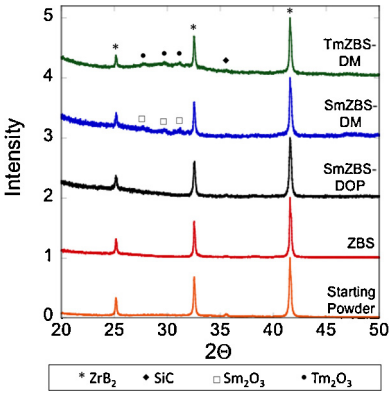

Fig. 2. X-ray scans of starting powders and as-sprayed coatings. Rare-earth oxide peaks are observed in SmZBS-DM and TmZBS-DM coatings between 2θ = 25–33°.

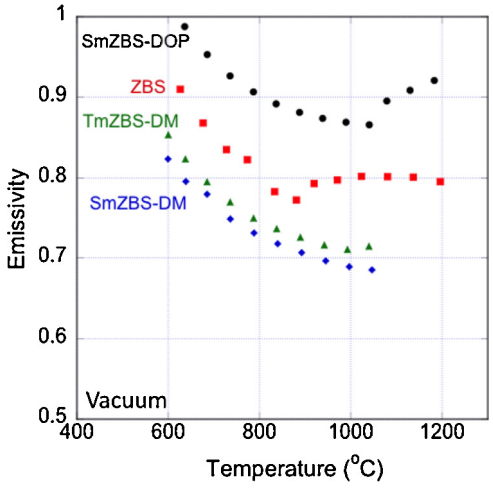

Fig. 3. The total hemispherical emissivity measured in a vacuum up to 1200 °C using ASTM C835-06 as a standard.

In this study, the high surface roughness of the SmZBS-DOP coating might increase its overall emissivity, but the difference in plateau temperatures (i.e. the local minimum in emissivity) undoubtedly indicates surface roughness alone is not enough to change the emissivity results. McMahon and Wilder also argued that the effect of surface roughness is negligible for thermal insulators.[9,23]

If surface roughness cannot explain the higher emissivity of the SmZBS-DOP coating compared to the SmZBS-DM coating, then the location of the samarium ion in the two coatings must be considered. XRD data for the SmZBS-DM (see Fig. 2) coating reveals that Sm_2O_3 powders are still present in crystalline form after plasma spraying. Neither samarium nor Sm_2O_3 was detected in the SmZBS-DOP coating via XRD, but samarium was detected by mass spectroscopy. Recall that Sm^{3+} was added to the coating by dissolving $Sm(NO_3)_3$ in ethanol and infiltrating the solution into the porous spray dried ZrB_2 powders. It is expected that Sm^{3+} would be predominantly located within the bulk of each ZrB_2 particle. The exact location of the Sm^{3+} within the ZrB_2 features is unknown but defects associated with its presence may strongly influence emissivity by changing its phonon and electron absorptions properties. Ultimately, a careful transmission electron microscopy (TEM) study is required to delineate differences in the microstructures of the SmZBS-DM and SmZBS-DOP coatings.

3.3. Thermal conductivity of plasma sprayed ZrB_2 composite

In addition to a high emissivity, a high thermal conductivity is also desired as it provides an alternative mechanism to conduct heat away from the narrow leading edge. The thermal conductivity of dense ZrB_2 with 30 vol.% SiC particulates between 400 °C and 1200 °C ranges between 55 and 64 W/m/K.[11] The thermal conductivity of Sm_2O_3 is not reported. However, dense rare-earth oxides have a thermal conductivity ranging from 2 to 15 W/m/K.[12] With this in mind, the thermal conductivity results for the SmZBS-DM, SmZBS-DOP, and ZBS coatings are presented in Fig. 4. The ZBS and SmZBS-DOP coatings have thermal conductivities of 2–4 W/m/K, clearly well below that of dense ZrB_2/SiC. The thermal conductivity of the SmZBS-DM coatings, ranging from 4 to 12 W/m/K, were higher than the SmZBS-DOP and ZBS coatings for all measured temperatures but still well below that of dense ZrB_2/SiC.

Microstructure and composition are some of the factors that influence the thermal conductivity of a coating. The large amount of porosity in the coatings greatly reduces the thermal conductivity. Assuming spherical porosity, the thermal conductivity for the ZBS sample with the measured porosity of 29.1 vol.% would be approximately 30.2–35.1 W/m/K.[24] As it is well established, the porosity in plasma-sprayed coatings is generally ellipsoidal in shape, with its long axis in the plane of the coating.[25] The shape factor of these pores further reduces the thermal conductivity compared to spherical pores.

Of interest in the current work is why the SmZBS-DM coating has a higher thermal conductivity than the ZBS coating. With similar lamellar microstructures and the fact that Sm_2O_3 would be expected to have a lower k_{th} than ZrB_2, its presence should not increase the k_{th} of the SmZBS-DM coating, but rather decrease it compared to the ZBS coating. However, inspection of Fig. 1a indicates that the distribution of pores in the ZBS coating is different than in the SmZBS-DM coating. While the SmZBS-DM coating contains a few large pores, the ZBS coating has smaller pores well distributed throughout the coating. The large pores reduce thermal conductivity in a coating but are less effective at reducing thermal conductivity than an equal volume fraction of pores well distributed in the coating.

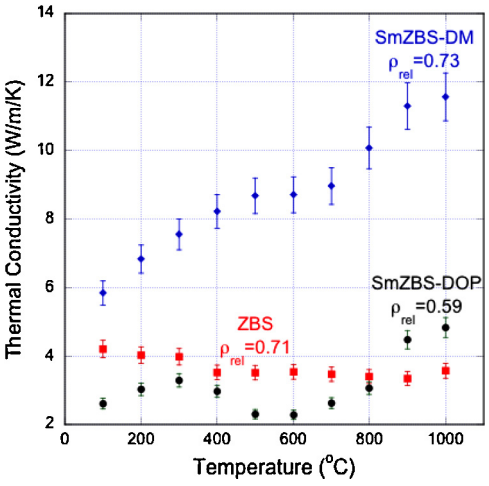

Fig. 4. The thermal conductivity of the coatings measured from 200 °C through 1000 °C using the laser flash technique.

While it is clear from the XRD data that the samarium in the SmZBS-DOP coating does not diffract, elemental analysis clearly demonstrated its presence. Despite having >10 vol.% more porosity than the ZBS coating, the k_{th} for the SmZBS-DOP coating was essentially the same for the pure ZBS coating. This can be accounted for with consideration of the shape of the porosity, which would tend to be more spherical in the SmZBS-DOP coating (see Fig. 1d), and therefore less effective at retarding heat flow than the more elliptical-shaped pores existing between lamellae expected in the ZBS coating.

3.4. Oxidation studies of ZBS-DM and ZBS-DOP coatings

3.4.1. Observations

Table 3 presents the XRD results from the surfaces of each coatings following oxidation at 900 °C, 1100 °C, and 1300 °C. Not apparent in this table was the amorphous hump observed at low 2θ for every coating composition and condition tested with some variation in thickness noted between coatings. As shown in Fig. 2 and Table 3 ZrB_2 and small amounts of α-SiC (less than 2 vol.%) were present in all coatings in the as-sprayed condition, with Sm_2O_3 and Tm_2O_3 detected in the SmZBS-DM and TmZBS-DM coatings, respectively.

m-ZrO_2 was detected in all the coatings after exposure at 900 °C. While α-SiC was noted in the ZBS coating after 900 °C exposure for 2 hours, this phase was not detected in any of the rare-earth modified coatings. Rare-earth borate phases were present after 900 °C exposure in all three of the rare-earth

Table 3
Phases present in as-sprayed and post heat-treated coatings identified by XRD. Amorphous humps were also detected at low 2θ.

	As-sprayed	900 °C	1100 °C	1300 °C
ZBS	ZrB_2 + α-SiC	*m*-ZrO_2 + α-SiC	*m*-ZrO_2	*m*-ZrO_2
SmZBS-DM	ZrB_2 + α-SiC + Sm_2O_3	*m*-ZrO_2 + $Zr(SiO_4)$ + $SmBO_3$ + $Sm(BO_2)_3$	*m*-ZrO_2 + $Zr(SiO_4)$	*m*-ZrO_2
SmZBS-DOP	ZrB_2 + α-SiC	*m*-ZrO_2 + $Sm(BO_2)_3$	*m*-ZrO_2	*m*-ZrO_2
TmZBS-DM	ZrB_2 + α-SiC + Tm_2O_3	*m*-ZrO_2 + $TmBO_3$	*m*-ZrO_2	*m*-ZrO_2

modified coatings, but did not contribute to the surface phase assemblage after the 1100 °C heat treatment. Differing from the other two rare-earth modified coatings, $Zr(SiO_4)$ was detected in the SmZBS-DM coating after the 900 °C and 1100 °C heat treatments. After a 1300 °C/2 hours heat treatment, only *m*-ZrO_2 and an amorphous hump on the surface of the samples was detected.

Fig. 6a shows the normalized weight gain as a function of temperature during heating of all four coatings investigated from 200 °C through 1300 °C. The ZBS coating demonstrated the lowest oxidation weight gain as compared to the rare-earth modified coatings. The ZBS coating shows upward inflections in weight gain at ~600 °C and ~1200 °C, consistent with temperature transitions reported by Bartuli et al. for ZrB_2/SiC coatings.[26] Similar to the ZBS coating, the rare-earth modified coatings also demonstrated increases in weight gain at ~600 °C and ~1200 °C, though sometimes the temperature transitions were shifted lower. The SmZBS-DOP coating demonstrated significantly higher weight gain than the DM coatings during the first upward deflection beginning at ~650 °C. Furthermore, the DM or DOP coatings all begin to exhibit weight loss at ~1200 °C, while the ZBS coatings continues to gain weight as noted by the positive slope of the normalized weight gain versus temperature plot.

The isothermal weight gain plots for 900 °C, 1100 °C, and 1300 °C are presented in Fig. 6b, c, and d. At 900 °C, the weight gains associated with the ZBS and two DM coatings were relatively similar, with the SmZBS-DOP coating demonstrating significantly higher weight gain. At 1100 °C, rapid oxidation rates were observed for both the SmZBS-DOP and TmZBS-DM coatings for the first 10 min. The weight gain data at 1300 °C indicates similar rapid oxidation for the first 10 min in the SmZBS-DM, TmZBS-DM, and SmZBS-DOP coatings. These coatings begin to lose weight after ~20 min, while the ZBS coating continues to gain mass with air exposure.

The isothermal normalized weight gain data was fitted with a para-linear function as described by:

$$w = K_{par}\sqrt{t} + K_{lin}t \quad (4)$$

where w is the normalized weight gain, K_{par} and K_{lin} are constants attributed to parabolic and linear weight changes, respectively, and t is time in minutes.[2] The K_{par} and K_{lin} constants are listed in Table 4 and have units of minute$^{-1/2}$ and minute^{-1}, respectively. K_{par} is always positive in the current study and attributed to oxidation, while K_{lin} is usually negative, indicative of a delayed oxidation process or mass loss from the surface due to glass evaporation process. Regression fitting using this para-linear law shows an excellent data match with R^2 ranges between 0.94 and 0.99 for all coatings evaluated.

The results in Table 4 indicate that for every coating investigated K_{par} increases with test temperature signifying that the oxidation kinetics increases with temperature. With the exception of the ZBS coating at 900 °C, where its K_{par} was slightly greater than the SmZBS-DM coating. This parameter was always less for the ZBS coatings compared to any of the rare-earth modified coatings. Negative K_{lin} values were observed in the SmZBS-DOP and TmZBS-DM coatings at 900 °C and 1100 °C. At 1300 °C, all coatings indicate a weight loss is occurring as evidenced by a negative K_{lin}. However, K_{lin}has a greater negative value in the rare-earth modified coatings than the ZBS coatings.

3.4.2. ZBS baseline behavior

Based on the phase analysis and microstructures in the current study, the ZBS oxidation results were similar to ZrB_2/SiC samples previously studied with the mechanistic reasons for the changes in weight are well understood.[26–28] The first weight gain inflections beginning near ~600 °C and observed in Fig. 6a can be attributed to oxidation of ZrB_2 to form porous *m*-ZrO2 and B2O3 glass. Consistent with this interpretation, Table 3 indicates that crystalline *m*-ZrO_2 was observed after 900 °C/2 h exposure and the presence of B_2O_3 glass was clearly observed in the ZBS surface at 900 °C (not shown). Below 1200 °C the underlying structure is protected by boria glass. Once the temperature exceeds 1200 °C, significant evaporation of B_2O_3 glass also begins to occur. SiC oxidizes to form SiO2 glass in the similar temperature range. Thus, the surface glass observed in Fig. 5a

Table 4
The K_{par} and K_{lin} constants for the presently studied coatings using a para-linear fit.

	K_{par}($\times 10^{-2}$ min$^{-1/2}$)	K_{lin} ($\times 10^{-2}$ min^{-1})
900 °C		
ZBS Baseline	0.7883	~0
SmZBS-DM	0.71	0.0049
SmZBS-DOP	2.2625	−0.0606
TmZBS-DM	1.2747	−0.0334
1100 °C		
ZBS Baseline	2.2562	~0
SmZBS-DM	3.09151	0.0039
SmZBS-DOP	5.6193	−0.18
TmZBS-DM	7.2454	−0.3195
1300 °C		
ZBS Baseline	5.071	−0.0914
SmZBS-DM	7.7914	−0.5234
SmZBS-DOP	7.2742	−0.4053
TmZBS-DM	8.3536	−0.5265

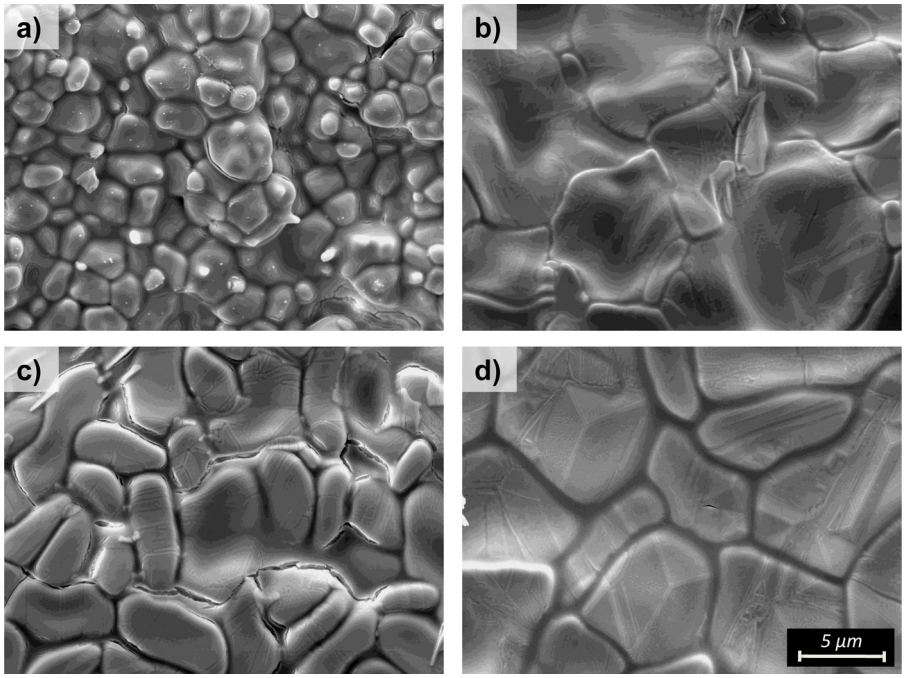

Fig. 5. SEM images of (a) ZBS, (b) SmZBS-DM, (c) SmZBS-DOP, and (d) TmZBS-DM coating surfaces after two hours exposure to flowing air at 1300 °C.

for the ZBS coating at 1300 °C is presumably rich in B_2O_3 with a small amount of SiO_2, ultimately forming a boria-rich borosilicate glass. Karlsdottir and Halloran noted that the viscosity of borosilicate glass decreases rapidly as the relative ratio of boria to silica increases.[29] While many studies have shown boria, silica, and borosilicate glass act to seal the surface of a porous structure to limit inward diffusion of oxygen,[30,31] the evaporation of the boria glass is responsible for weight loss. In the current study, the weight loss observed in the ZBS coatings at 1300 °C, as indicated by the small K_{lin} value of -0.0914×10^{-2} min^{-1} was attributed to evaporation of the boria in the surface glass. It should be noted that the oxidation resistance of the coatings is not optimized because most of the SiC intended for the coatings was not successfully incorporated into the coating. The following discussion will compare the oxidation behavior of the rare-earth modified coatings to the ZBS coatings at 900 °C, 1100 °C, and 1300 °C.

3.4.3. Rare-earth modified coatings at 900 °C

Referring to Fig. 6a and b, the dramatic weight gains associated with the SmZBS-DOP coatings can be attributed to the oxidation of samarium into $Sm(BO_2)_3$, one of the reaction products shown in Table 3. The weight gain behavior of the SmZBS-DM and TmZBS-DM coatings at 900 °C was similar to the ZBS coating. However, the XRD results indicate that rare-earth borates were formed, as well as $Zr(SiO_4)$, in the SmZBS-DM coating. The formation of $Zr(SiO_4)$ at this temperature was also observed by Bartuli et al.[26] From Fig. 6b the formation of these crystalline compounds is not greatly affecting the weight gain behavior of the two DM coatings relative to the ZBS coating. The rare-earth additions were already oxidized (as Sm_2O_3 or Tm_2O_3) prior to beginning the test and this could explain the weight gain differences noted between the DM and SmZBS-DOP coatings. Inspection of the oxidized surfaces of the rare-earth modified coatings after a 900 °C/2 h exposure suggest the presence of a B_2O_3 glass. However, this boria did not have the same composition as the surface glass in the ZBS coating, as Sm^{3+} or Tm^{3+} was detected in the glass phase via EDS. The K_{lin}data found in Table 4 for the SmZBS-DOP and TmZBS-DM coatings was slightly negative at 900 °C. As boria does not evaporate at 900 °C, the negative K_{lin}at this temperature is attributed to delayed parabolic oxidation due to the glassy layer acting as a rate-limiting step.

The XRD results in Table 3 indicate that the α-SiC that was previously detected in the as-sprayed condition is not there. With the knowledge that SiC does not oxidize at this low a temperature,[26–28] it is not thought that the SiC has begun to oxidize in the coatings studied presently. Its absence from the XRD results is likely a consequence of the small amount of SiC in the coatings and the formation of a surface glassy layer that would further minimize its diffraction intensity.

3.4.4. Rare-earth modified coatings at 1100 °C

Only *m*-ZrO_2 is observed in the coatings, except for traces of $Zr(SiO_4)$ in the SmZBS-DM sample. It is not clear why this phase forms and is detectable in this coating and not in the other two rare-earth modified coatings. The ZrO_2-SiO_2 phase diagram suggests that $Zr(SiO_4)$ should be stable up to 1676 °C.[32] However, the $Zr(SiO_4)$ is only detected up to 1100 °C, evidently due to the presence of impurities such as

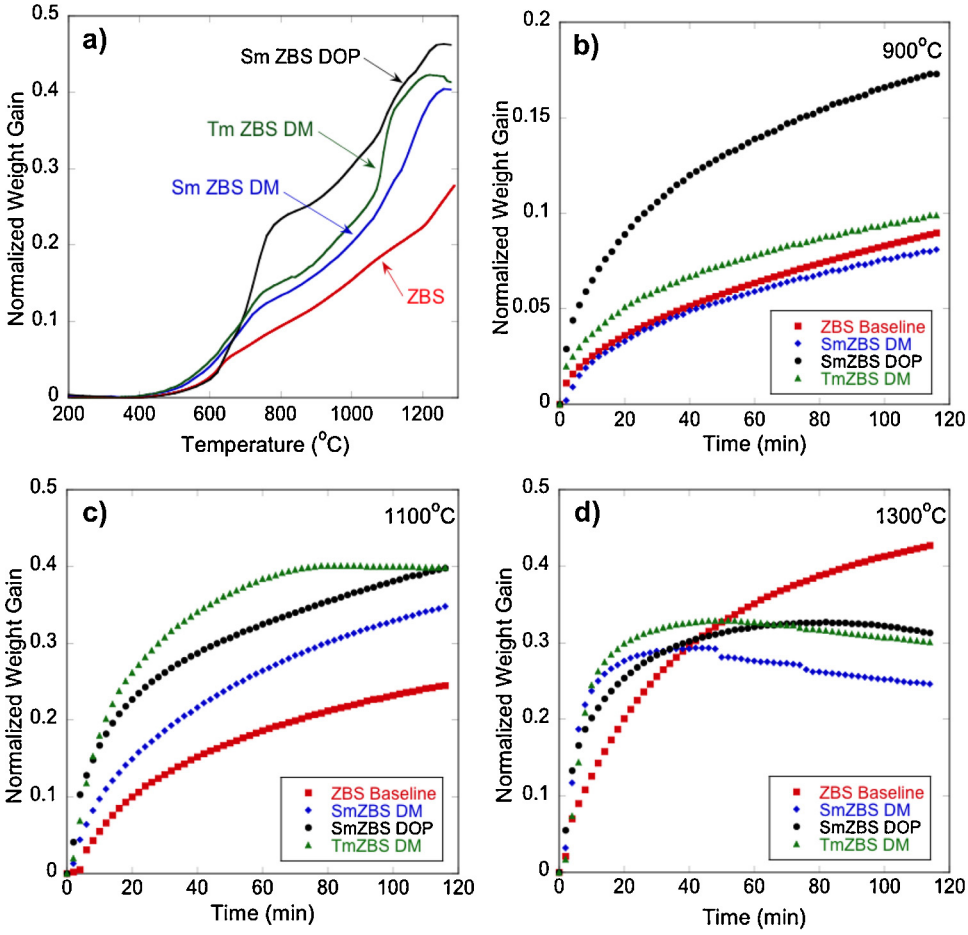

Fig. 6. Weight gain data for all four coatings at (a) 200–1300 °C; isothermal (b) 900 °C; (c) 1100 °C; and, (d) 1300 °C with 100 sccm flowing air. ZBS coating demonstrated the lowest oxidation rate compared to the rare-earth modified coatings.

the rare-earth elements which act to decrease its decomposition temperature.[33]

SiC was not detected in any of the coatings after a 2 h exposure at 1100 °C. Again, the low concentration of SiC (1.7 vol.%) is hard to detect via XRD. As shown in Fig. 6c, the weight gain behavior at 1100 °C of all the rare-earth modified coatings is greater than the ZBS coating. Fig. 6a indicates a significant change in the normalized weight gain slope near 1100 °C for all rare-earth modified coatings, while the ZBS coating does not show a significant difference until reaching 1200 °C.

It is known that the presence of rare-earth ions disrupts the perfect tetrahedron or planar structure of silica and boria. These lower the melting temperature and viscosity of the glass.[34,35] In the current study, boria glass is believed to begin evaporating at ~1100 °C as evidenced by the negative values of K_{lin} for the SmZBS-DOP and TmZBS-DM coatings. Therefore, there are two possible reasons for higher K_{par} and lower K_{lin} in the rare-earth modified coatings. First, based on the Stoke–Einstein relation and Eyring viscosity equation, the low viscosity glass has a higher oxygen diffusion rate, causing more underlying ZrB_2 and SiC to oxidize.[36] Second, due to the lower viscosity and melting temperature the boria-rich borosilicate glass evaporates at ~1100 °C, leaving the surface unprotected. The TmZBS-DM coating demonstrated a plateau in the normalized weight gain after 70 min into the test, indicative that the surface of the coating is oxidizing as quickly as the thulium modified glass is evaporating.

3.4.5. Rare-earth modified coatings at 1300 °C

Only *m*-ZrO_2 was detected on the surface of the samples even though Fig. 5b, c and d show that a glassy phase is still present on the surface. Fig. 6d shows significant weight loss in the rare-earth modified coatings. It is noteworthy that the K_{lin} values for the rare-earth modified coatings are approximately four times more negative than for the ZBS coating, indicating significant evaporation for these coatings at this temperature. Thus, it appears that the rare-earth additions are modifying the boria glass.

Finally, assuming all the SiC in the coating oxidized to SiO_2, its effects toward oxidation resistance is minimal and should be considered negligible. It is speculated that if 20 vol% SiC were to be present in the rare-earth modified coatings, the weight lost, or K_{lin} will be less significant because of the formation of higher viscosity and lower oxygen permeability SiO_2 glass on the oxidized surface.

3.4.6. Summary of oxidation results

Though the phases and topographies are similar for the rare-earth modified and ZBS coatings at 1100 °C and 1300 °C, their behavior in an oxidizing atmosphere differs. It is clear that as temperature increases, rare-earth ion modification of the boria glass increases its evaporation rate. This is likely an undesirable result for the rapid flow rates associated with hypersonic flight. However, the coatings formed for the present study represent the first generation of high emissivity coatings and improvements in processing and design are expected. Specifically, increasing the amount of SiC in the final rare-earth modified coatings should increase the oxidation resistance of these coatings. Furthermore, the oxidizing experiments currently performed were static and the effect of non-equilibrium heating expected during hypersonic flight would likely alter the results.

4. Conclusions

ZrB_2/SiC and rare-earth-modified ZrB_2/SiC coatings were fabricated via shrouded air plasma spray. Two approaches were taken to incorporate the rare-earth oxide (REO) or ion into coatings of ZrB_2/SiC. In the first approach, Sm_2O_3 or Tm_2O_3 powders were added to spray-dried ZrB_2 powders and SiC powders via dry mechanical mixing. In the second approach, a $Sm(NO_3)_3$ solution was infiltrated into spray dried ZrB_2 powders with SiC powders added. Lamella formation was observed in coatings fabricated from dry mixed powders, while the microstructural features in the doped coatings indicated the powders were only partially melted. Based on x-ray diffraction and mass spectroscopy results, rare-earth elements were successfully integrated into the coatings as either oxides (for the dry mixed coatings) or ions (for the doped coating).

It was clear from this study that rare-earth elements have the ability to modify emissivity. However, the method used to incorporate rare-earth elements into the ZrB_2/SiC coating has a significant effect on emissivity. The emissivity of SmZBS-DOP coating is approximately 10% higher than that of ZBS coating and 18% higher than that of SmZBS-DM coating. The porous ZBS and rare-earth modified coatings have thermal conductivities of 2 to 12 W/m/K, well below that of dense ZrB_2/SiC.

Finally, the presence of rare-earth elements in the coatings affects the boria-rich surface glass formed during oxidation as evidenced by differences in evaporation rate between ZBS and rare-earth modified ZBS coatings. Processing improvements to increase the amount of SiC in the final coating will help to reduce these effects.

Acknowledgements

The authors acknowledge Praxair Surface Technologies for providing access to the plasma spray facilities and financial support from Dr. Ali Sayir of Air Force Office of Scientific Research (AFOSR Grant# FA9550-11-1-0079). The authors are also grateful for helpful discussion on band structures of rare-earth oxides with Prof. Alejandro Strachan and Dr. Stanislav Avdoshenko. The thermal conductivity test was supported by the assistant secretary of Energy Efficiency and Renewable Energy of DOE through the Vehicle Technology Program and the High Temperature Materials Laboratory user program of ORNL managed by the UT-Battelle LLC, for the Department of Energy under contract DE-AC05000OR22725.

References

1. Van Wie DM, Drewry DG, King DE, Hudson CM. The hypersonic environment: required operating conditions and design challenges. *J Mater Sci* 2004;**39**(19):5915–24.
2. Monteverde F. The thermal stability in air of hot-pressed diboride matrix composites for uses at ultra-high temperatures. *Corros Sci* 2005;**47**:2020–33.
3. Tului M, Marino G, Valente T. Plasma spray deposition of ultra high temperature ceramics. *Surf Coat Technol* 2006;**201**:2103–8.
4. Squire TH, Marschall J. Material property requirements for analysis and design of UHTC components in hypersonic applications. *J Eur Ceram Soc* 2010;**30**:2239–51.
5. Bertin JJ, Cummings RM. Fifty years of hypersonics: where we've been, where we're going. *Prog Aerosp Sci* 2003;**39**:511–36.
6. Guazzoni GE. High-temperature spectral emittane of oxide of erbium, samarium, neodymium and ytterbium. *Appl Spectrosc* 1972;**26**(1):60–5.
7. Alfano D, Scatteia L, Cantoni S, Balat-Pichelin M. Emissivity and catalycity measurements on SiC-coated carbon fibre reinforced silicon carbide composite. *J Eur Ceram Soc* 2009;**29**:2045–51.
8. Blair R. Determination of spectral emissivity of ceramic bodies at elevated temperatures. *J Am Ceram Soc* 1960;**43**(4):197–203.
9. McMahon WR, Wilder DR. Hemispherical spectral emittance of selected rare earth oxides. *J Am Ceram Soc* 1968;**51**(4):187–92.
10. Gol'danskii VI. The periodic system of D. I. Mendeleev and problems of nuclear chemistry. *J Chem Educ* 1970;**46**(6):406.
11. Zimmermann JW, Hilmas GE, Fahrenholtz WG, Dinwiddie RB, Porter WD, Wang H. Thermophysical properties of ZrB2 and ZrB2–SiC ceramics. *J Am Ceram Soc* 2008;**91**:1405–11.
12. Metals and Ceramics Information Center. Engineering Property Data on Selected Ceramics, Single Oxides. *MCIC-HB-07*, Vol. III; 1981.
13. M. Tului, T. Valente. Process for the manufacturing of ceramic-matrix composite layers and related composite material. U.S. Pat. Appl. Publ., US 2002/0151427; 2002.
14. Tului M, Lionetti S, Pulci G, Rocca E, Valente T, Marino G. Effects of heat treatments on oxidation resistance and mechanical properties of ultra high temperature ceramic coatings. *Surf Coat Technol* 2008;**202**(18):4394–8.
15. Pulci G, Tului M, Tirillo J, Marra F, Lionetti S, Valente T. High temperature mechanical behavior of UHTC coatings for thermal protection of re-entry vehicles. *J Therm Spray Technol* 2011;**20**(1/2):139–44.
16. ASTM C373-88. *Standard Test Method for Water Absorption, Bulk Density, Apparent Porosity, and Apparent Specific Gravity of Fired Whiteware Products*. ASTM International; 2006.
17. ASTM C835-06. *Standard Test Method for Total Hemispherical Emittance of Surfaces up to 1400 °C*. ASTM International; 2006.
18. ASTM E1461-11. *Standard Test Method for Thermal Diffusivity by the Flash Method*. ASTM International; 2006.
19. Thermophysical Properties of Matter Database (TPMD), CINDAS LLC, Ver. 8, 2012.
20. Pawlowski L. *The Science and Engineering of Thermal Spray Coatings*. Hoboken, NJ: John Wiley & Sons; 1995.
21. Tului M, Ruffini F, Arezzo F, Lasisz S, Znamirowski Z, Pawlowski L. Some properties of atmospheric air and inert gas high-pressure plasma sprayed ZrB_2 coatings. *Surf Coat Technol* 2002;**151/152**:483–9.
22. S. Avdoshenko, A. Strachan, "Stain Enhancement of High-k Dielectric Response in $(La/Sc)_2O_3$ and $LaScO_3$: An ab-initio Study," unpublished results.
23. Scatteia L, Alfano D, Monteverde F, Sans J-L, Balat-Pichelin M. Effect of the machining method on the catalycity and emissivity of ZrB_2 and ZrB_2–HfB_2-based ceramics. *J Am Ceram Soc* 2008;**91**(5):1461–8.

24. Kingery WD, Bowen HK, Uhlmann DR. *Introduction to Ceramics*. 2nd ed. New York: John Wiley and Son, Inc.; 1976.
25. Ilavsky J, Allen AJ, Long GG, Krueger S, Berndt CC, Herman H. Influence of spray angle on the pore and crack microstructure of plasma-sprayed deposits. *J Am Ceram Soc* 1997;**80**(3):733–42.
26. Bartuli C, Valente T, Tului M. Plasma spray deposition and high temperature characterization of ZrB_2-SiC protective coatings. *Surf Coat Technol* 2002;**155**(2/3):260–73.
27. Monteverde F, Bellosi A. Oxidation of ZrB_2-based ceramics in dry air. *J Electrochem Soc* 2003;**150**(11):B552–9.
28. Rezaie A, Fahrenholtz WG, Hilmas GE. Evolution of structure during the oxidation of zirconium diboride-silicon carbide in air up to 1500 °C. *J Eur Ceram Soc* 2007;**27**(6):2495–501.
29. Karlsdottir SN, Halloran JW. Oxidation of ZrB_2–SiC: influence of SiC content on solid and liquid oxide phase formation. *J Am Ceram Soc* 2009;**92**(2):481–6.
30. Sarin P, Driemeyer PE, Haggerty RP, Kim D-K, Bell JL, Apostolov ZD, et al. In situ studies of oxidation of ZrB_2 and ZrB_2–SiC composites at high temperatures. *J Eur Ceram Soc* 2010;**30**:2375–86.
31. Sciti D, Brach M, Bellosi A. Oxidation behavior of a pressureless sintered ZrB_2–$MoSi_2$ ceramic composite. *J Mater Res* 2005;**20**(4):922–30.
32. Butterman WC, Foster WR. Zircon stability and the ZrO_2–SiO_2 phase diagram. *Am Mineral* 1967;**52**:880–5.
33. Kaiser A, Lobert M, Telle R. Thermal stability of zircon ($ZrSiO_4$). *J Eur Ceram Soc* 2008;**28**:2199–211.
34. Doremus RH. *Glass Science*. New York: John Wiley & Sons; 1994.
35. Eakins E, Jayaseelan DD, Lee WE. Toward oxidation-resistant ZrB_2-SiC ultra high temperature ceramics. *Metallurgical Mater Transact A* 2011;**42**:878–87.
36. Karlsdottirw SN, Halloran JW. Formation of oxide scales on zirconium diboride–silicon carbide composites during oxidation: relation of subscale recession to liquid oxide flow. *J Am Ceram Soc* 2008;**99**(11):3652–8.